Wind-Induced Response of a Roof Purlin

by

Jianming Yin[1], Douglas A. Smith[2] and Kishor C. Mehta[3]

ABSTRACT

The proper orthogonal decomposition (POD) technique is used to estimate the fluctuating response of a roof purlin on the Texas Tech University full-scale test building. The contribution of the first three eigenvalues to the total energy is calculated and agrees with the wind tunnel results. The accuracy of the reconstruction of the pressure time series is investigated. The static and fluctuating response coefficients for pressure taps are calculated and compared in this paper.

KEYWORDS: full-scale test; proper orthogonal decomposition (pod) technique; purlin; wind-induced response

1. INTRODUCTION

Low-rise buildings are immersed in the near-ground flow field and usually experience higher turbulent flows than high-rise buildings. The turbulence intensity of the approaching flow has significant effects on the peak values of wind pressure, and thus the peak wind loading on the building envelope, especially on the roof area (Cochran et al., 1992). The quasi-steady theory indicates that high turbulence in the approach flow results in high turbulence in wind pressures on a building (Cook, 1990). Therefore, for low-rise buildings, a relatively high fluctuating response of their structural components is expected. In fact, field measurements of purlin deflections on the test building of the Wind Engineering Research Field Laboratory (WERFL), Texas Tech University (TTU) verifies this expectation (Bhavaraju, 1993, Smith et al., 1994).

The static response of the purlin was studied by (Bhavaraju, 1993). In this paper, only the fluctuating response of the purlin is investigated using the Proper Orthogonal Decomposition (POD) technique. The contribution of the first three eigenvalues is obtained. The reconstruction of the pressure time series using the first three eigenvalues is conducted and the accuracy of the reconstruction for pressures at different locations is discussed. The fluctuating response coefficients for pressure taps in the effective area of a purlin are obtained and compared with the static response coefficients.

2. EXPERIMENTAL SETUP

The instrumentation and data acquisition system of the Wind Engineering Research Field Laboratory (WERFL) at TTU have been described in detail by Levitan et al. (1992). A brief description related to this experiment is given here.

The location of the purlin used for this investigation, the designation of pressure taps in the purlin's effective area, (numbered from G10 to G15) and the definition of angle of attack of wind on the building are shown in Figure 1.

---

[1]Research Assistant, Department of Civil Engineering, Texas Tech University, Lubbock, Texas, 79409-1023, USA

[2]Research Assistant Professor, Department of Civil Engineering, Texas Tech University, Lubbock, Texas, 79409-1023, USA

[3]P.W. Horn Professor, Department of Civil Engineering, Texas Tech University, Lubbock, Texas, 79409-1023, USA

This instrumented 25 ft (7.62m) long Z-shaped purlin is simply supported with a 1'-4" (0.41m) overhang adjacent to the wall. Six pressure taps are placed in the effective area of the purlin. Differential pressure transducers are used to measure the pressures at the taps. These transducers are referenced to atmospheric pressure from an underground box (Levitan, 1993). The sampling rate for building surface pressures is 40 Hz.

Two Direct Current Displacement Transducers (DCDT) manufactured by Trans-Tek Incorporated are used for monitoring the midspan deflection of purlin. The DCDTs have a flat frequency response to 20 Hz. The DCDTs are sampled at 10 Hz and filtered at 8 Hz (Smith et al., 1994). The static influence coefficient surface for the purlin was developed experimentally by Bhavaraju (1993) and is shown in Figure 2.

3. PROPER ORTHOGONAL DECOMPOSITION (POD) TECHNIQUE

Wind pressure distribution over the effective area of a structural member is a function of both time and space, say $p(x,y,t)$. The spatio-temporal random characteristics of wind pressure, and thus wind loading, make it difficult to evaluate or predict the fluctuating response of a structure or a member. One technique used to predict the response of structural members to wind loads is the Proper Orthogonal Decomposition (POD). The POD technique decomposes a spatio-temporal random function of wind pressure, $p(x,y,t)$, into several deterministic distributions, $\Phi_i(x,y)$'s, and their associated temporal function or principal coordinates, $a_i(t)$'s. The detailed description of this technique can be found in Loeve (1977). A brief description of the POD technique is given here.

Given simultaneously recorded time series at pressure taps which are uniformly distributed over an area, $p(x_1,y_1,t)$, $p(x_2,y_2,t)$, ..., $p(x_N,y_N,t)$, the covariance, R_{ij}, for each pair of these series at zero time lag can be obtained as:

$$R_{ij}=\int_T p(x_i,y_i,t)p(x_j,y_j,t)dt \qquad (1)$$

where T is the record length.

When $i=j$, the result of the above equation is the autocovariance of $p(x_j,y_j,t)$. Using these covariance values, a real symmetric covariance matrix $[R_{ij}]$ of the order of $N\times N$ can be established. The eigenvectors and eigenvalues of this matrix are determined and the principal coordinate can be computed using:

$$a_i(t)=\frac{\sum_{k=1}^{N} p(x_k,y_k,t)\Phi_i(x_k,y_k)}{\Phi_i^2(x_k,y_k)} \qquad (2)$$

where:
$\Phi_i(x,y)$ is the i^{th} eigenvector; and,
$a_i(t)$ is the i^{th} principal coordinate.

From the definition of $a_i(t)$, it is shown that the principal coordinates are orthogonal. The eigenvectors, which are orthogonal to each other, give the common distributions of wind pressures over an area while the related eigenvalues indicate the relative weighting contributed by their associated eigenvectors.

The original pressure, $p(x,y,t)$, can be decomposed using a set of known eigenvectors and principal coordinates as:

$$p(x_i,y_i,t)=\sum_{k=1}^{N} a_k(t)\Phi_k(x_i,y_i) \qquad (3)$$

For the case under consideration, Eq. 3 can be simplified to:

$$p(x_i,t)=\sum_{k=1}^{N} a_k(t)\Phi_k(x_i) \qquad (4)$$

where:
$a_k(t)$ is k^{th} principal coordinate, and,
$\Phi_k(x_i)$ is i^{th} component of k^{th} eigenvector.

Using the POD technique, Best et al. (1983), Bienkiewicz et al. (1992), Holmes (1990), and Ho (1992) presented, respectively, their results by analyzing pressure data from wind tunnel tests.

3.1 Contribution of eigenvectors

The wind pressure data on the purlin collected at the test building of WERFL are used to construct a covariance matrix. To make the results reasonably comparable with those from wind tunnel tests (Best et al, 1983, Bienkiewicz et al, 1992, Holmes, 1990), only five pressure taps, G10, G11, G12, G14 and G15 are used in order to make the spacing of pressure taps as uniform as possible.

For this work, net pressures across the roof envelope are used. Internal pressure inside the TTU test building is uniform (Yeatts et al., 1993). The external pressure is assumed to be uniformly distributed over the tributary area shown in Figure 3. The net pressure coefficient for the tributary area associated with a specific pressure tap is:

$$C_{PN}(t)=C_{PE}(t)-C_{PI}(t) \quad \text{(downward positive)} \quad (5)$$

where the pressure coefficient, C_p is defined as follows:

$$C_p(t)=\frac{p(t)}{0.5\rho V^2} \quad (6)$$

where:
$p(t)$ is wind pressure;
ρ is air density; and,
V is the mean wind speed averaged over 15 minutes measured at roof height.

Records with the angle of attack approximately equal to 0°, 20°, 315° and 270° are selected for analysis. The calculated results listed in Table 1 show that the first three eigenvalues constitute 80% or more of total energy. The first eigenvalue is typically 50% of the total energy. The results have a good agreement with these from wind tunnel tests by Best et al. (1983). While the contribution of the first eigenvalue in this study is less compared to the results by Bienkiewicz et al. (1992).

3.2 Reconstruction of pressure history

Pressure coefficient time histories can be decomposed using a complete set of orthogonal eigenvectors used as base functions. A limited number of these eigenvectors can be used to reconstruct a new pressure history that approximates the original one. If a complete set of eigenvectors is used, the reconstructed time history will be equal to the original one. In most cases, to ensure the precision of reconstruction and to reduce the calculations, only the first three eigenvectors are used. For this study, the first three eigenvectors account for 80% or more of the total energy, thus the time history is reconstructed using only the first the three eigenvectors.

Fig. 4 shows the original and reconstructed time histories using the first three eigenvalues for record M15N609. The original pressure coefficient histories for G11 and G15 are plotted on the left side and the corresponding reconstructed one on the right side. Pressure taps G11 is, for this angle of attack (23.6°), in the separation bubble and G15 is in the reattachment region.

A comparison of the mean and standard deviation show a good match for tap G11. However there is a significant difference in the couple for tap G15. The cross correlation coefficients of each couple for G11 and G15 are 0.9997 and 0.361 respectively. This implies the accuracy of pressure reconstruction may depend upon the location of a pressure tap.

3.3 Prediction of fluctuating response coefficients of purlin

As mentioned, the purlin deflection was monitored simultaneously along with the surface point pressure in the purlin's effective area. These data can be used to evaluate the fluctuating response characteristics of the purlin to fluctuating wind loads.

The expression for the relationship between the wind pressures acting on a component and the response of the component can be found in Holmes (1990). The static and fluctuating response coefficient for a purlin may not be the same. The equations for static and fluctuating response are:
For static response:

$$\overline{W} = \sum_{k=1}^{N} \eta_k \overline{C}_{pk} A_k q \qquad (7)$$

For fluctuating response:

$$W(t) = \sum_{k=1}^{N} \lambda_k C_{pk}(t) A_k q \qquad (8)$$

where:
$\overline{W}$ and $W(t)$ are the mean and fluctuating component of purlin response;
$\overline{C}_{pk}$ and $C_{Pk}(t)$ are the mean and fluctuating component of a pressure coefficient at tap k;
η_k and λ_k are the static and fluctuating response coefficients of the purlin due to the mean and fluctuating pressure at tap k;
A_k is the tributary area associated with the specific pressure measurement at tap k (under the assumption that $p_k(t)$ is uniformly acting on A_k); and,
q is velocity pressure.
The evaluation method to determine the static purlin response is given by Bhavaraju (1993). The fluctuating response is considered below.

The displacement response of the purlin and the pressure coefficient time histories at taps, numbered G10 through G15, have been measured. For simplicity, the 5 taps are renumbered 1 to 5 instead of G10, G11, G12, G14 and G15, respectively.

Multiplying both sides of Eq. 8 by C_{pj} $(j=1,...5)$ and integrating, we obtain:

$$\int_0^T W(t) C_{pj}(t) dt = \sum_{k=1}^{5} \int_0^T \lambda_k C_{pk}(t) C_{pj}(t) A_k q dt \qquad (9)$$

where T is the record length. In this case T=900 sec.

Introducing the concept of the covariance function, Eq. 9 can be rewritten as:

$$COV(W, C_{pj}) = \sum_{k=1}^{5} \lambda_k A_k q COV(C_{pk}, C_{pj}) \qquad (10)$$

Where $COV(\bullet, \bullet)$ is the value of covariance function at time lag $\tau=0$.

Using these five pressure taps, $j=1,...,5$, five simultaneous equations are established with five unknowns, i.e. fluctuating response coefficients, λ_1 to λ_5. These equations are solved for the λ_i's. The results are shown in Table 2 along with the static influence coefficient.

The fluctuating coefficient, λ_i, usually is not equal to the static coefficient, η_i, and appears to be a function of the angle of attack. For records with similar angles of attack, e.g., 609 and 611($\alpha \approx 20^0$), or 728 and 730($\alpha \approx 4^0$), the fluctuating coefficients have slight difference. This difference may be caused by the differences in longitudinal and lateral turbulence intensities. This difference may also be caused by the response characteristics of the purlin. Figures 5 and 6, taking record M15N609 as an example, demonstrate the comparison of the normalized spectral density functions of the purlin response and local pressures. It is found, from the figures, that the purlin response usually lose some magnitude in the relatively high frequency domain

starting from 0.3 Hz ($\log_{10}0.3\approx-0.5$) compared to the spectral functions of local pressure. From Table 2, it can be observed that the fluctuating response coefficients are the function of the angle of attack. For example, records 728 and 730, with the angle of attack approximately equal to 0°, the fluctuating response coefficients are higher than those for records 609 and 611 ($a\approx20°$) which are higher than those of records 795 ($a\approx315°$, or so-called quartering wind).

Another reason for the difference between static and fluctuating response coefficient is the assumption that the pressure measured at the tap represents the pressure on the whole tributary area. When an oncoming flow is attacking at the direction of 0°, a high-suction bubble enhances the correlation of wind pressure along the width of the purlin. The correlation will decrease as an acting wind skews from normal direction; thus the actual net effect of wind pressure on a tributary area should be lower than the wind pressure measured at a single point because the low correlated pressure components cancel out each other. This so-called area-averaging effect may be one of the factors that cause the fluctuating response coefficient to be lower than the static one.

3.4 Prediction of purlin response using both original and reconstructed pressure histories

Based on the analysis in section 3.2, the reconstructed pressure history, using the first three or more eigenvectors, can be used to approximate the original one. The precision of this reconstruction depends on how many eigenvectors have been used and the location of the pressure tap. The reconstructed histories are used here to predict the purlin response.

In practice, structural response such as support reaction, deflection and bending moment of a member, is of primary concern for engineers for design. Therefore instead of the wind pressures, it is actually the precision of the estimated structural response that determines how many eigenvectors should be used to reconstruct pressures. In this case, since the fluctuating response coefficients, λ_i's ,have been obtained in section 3.3, Eq. 8 can be used to predict purlin response. By substituting original and reconstructed pressure histories into Eq. 8, respectively, two predicted purlin deflection histories for each record are obtained. The standard deviations and ranges of two predicted histories are listed in Table 3 along with the measured response for comparison purposes. The results show a good agreement. Therefore, in this case the first three eigenvectors are sufficient to be used to predict purlin deflection and thus the pressure coefficients.

4. CONCLUSIONS

1) The results obtained from the field measurements at WERFL, Texas Tech show that the first three eigenvalues usually constitute up to 90% of the total energy while the first one alone accounts for 50% or more.

2) The fluctuating response coefficient is different from the static one.

3) Spectral analysis shows that purlin deflection loses some magnitude in the high frequency range.

4) The reconstructed pressures using the first three principal coordinates may be used to estimate the fluctuating response of the purlin.

5. ACKNOWLEDGMENT

The assistance provided by Mr. S.V. Bhavaraju in analysis effort is appreciated. The appreciation also goes to the Wind Engineering Research Field Laboratory team who made available the excellent wind pressure data. The financial support by the National Science Foundation (Grant BCS-8821163) and the Metal Building Manufacturer's Association are gratefully acknowledged by the writers.

6. REFERENCES

Best, R.J. and Holmes, J.D. (1983), "Use of Eigenvalues in the Covariance Integration Method for Determination of Wind Load Effects", Journal of Wind Engineering and Industrial Aerodynamics, Vol. 13, pp 359-370, Elsevier.

Bhavaraju, S.V. (1993), "Wind-Induced Pressures on a Roof Purlin", Master's Thesis, Department of Civil Engineering , Texas Tech University, Lubbock, Texas.

Bienkiewicz, B., Hee-Jung, H., and Sun, Y. (1992), " Proper Orthogonal Decomposition of Roof Pressure", BBAA2, Australia.

Cochran, L.S. and Cermak, J.E. (1992), "Full- and Model-Scale Cladding Pressure on Texas Tech University Experimental Building", Journal of Wind Engineering and Industrial Aerodynamics, Vol 41-44, pp 1589-1600, Elsevier.

Cook, N.J. (1990), "The Designer's Guide to Wind Loading of Building Structures", Part 2, Static Structures, Butterworths, London.

Ho, T.C.E. (1992), "Variability of Low Building Wind Loads", Ph. D. Dissertation, Department of Civil Engineering, Faculty of Engineering Science, The University of Western Ontario, London.

Holmes, J. D. (1990), "Analysis and Synthesis of Pressure Fluctuations on Bluff Bodies Using Eigenvectors", Journal of Wind Engineering and Industrial Aerodynamics, Vol.33, pp 219-230, Elsevier.

Levitan, M.L. (1993), "Analysis of Reference Pressure Systems Used in Field Measurements of Wind Loads", Ph.D. Dissertation, Department of Civil Engineering, Texas Tech University, Lubbock, Texas.

Levitan, M.L. and Mehta, K.C. (1992), "Texas Tech Field Experiments for Wind Loads parts I and II" , Journal of Wind Engineering and Industrial Aerodynamics, Vol.41-44, pp 1565-1588, Elsevier.

Loeve, M. (1977), "Probability Theory I", 4th Edition, Springer-Verlag Inc., New York.

Smith, D.A. (1993), "Stochastic Analysis of Wind Data", Ph. D. Dissertation, Department of Civil Engineering, Texas Tech University, Lubbock, Texas.

Smith, D.A., Mehta, K.C., Yeatts, B.B. and Bhavaraju, S.V. (1994), "Area-Averaged and Internal Pressure Coefficients Measured in the Field", Accepted for publication in the Journal of Wind Engineering and Industrial Aerodynamics.

Yeatts, B.B. and Mehta, K.C. (1993), "Field Experiments for Building Aerodynamics" Journal of Wind Engineering and Industrial Aerodynamics, Vol. 50, pp 213--224, Elsevier

Table 1. Contribution by First Three Eigenvalues

Eigenvalue	Run No. Mode 15						
	609	611	728	730	542	544	795
1st	56%	59%	53%	59%	42%	49%	81%
2nd	17%	16%	20%	23%	20%	20%	10%
3rd	16%	15%	16%	10%	15%	13%	4%
Sum	89%	90%	89%	92%	80%	82%	95%

Table 2. Fluctuating and Static Response Coefficients

Run No.	Angle of attack, θ	I_u	I_v	U	λ_k				
					G10	G11	G12	G14	G15
609	23.6°	0.161	0.139	22.7	0.105	0.084	0.173	0.192	0.046
611	20.1°	0.175	0.151	22.5	0.077	0.079	0.179	0.214	0.064
728	3.9°	0.191	0.180	16.5	0.115	0.148	0.307	0.276	0.080
730	4.9°	0.213	0.153	18.5	0.093	0.146	0.313	0.333	0.035
542	260.2°	0.201	0.150	20.0	0.051	0.087	0.081	0.100	0.064
544	266.5°	0.167	0.201	21.8	0.100	0.100	0.112	0.109	0.068
795	314^0	0.223	0.188	18.1	0.053	0.043	0.114	0.039	0.102
		Static	Coef.	η_k	0.095	0.334	0.555	0.430	0.137

Note: I_u and I_v denote longitudinal, lateral turbulence intensity, respectively; and,
U denotes mean wind speed (mph).

Table 3. Comparison of Predicted and Measured Purlin Response ($\times 10^{-3}$ in.)

	609		611		542		544	
	std	range	std	range	std	range	std	range
meas	8.26	51.9	8.95	53.7	6.89	49.6	8.43	69.6
pred1	7.65	56.6	6.95	46.3	6.13	44.5	7.53	50.0
pred2	7.06	50.4	8.70	6.69	5.98	43.5	7.36	59.1

Note: 'meas' denotes the measured purlin response;
'pred1' denotes the predicted purlin response by original pressure histories; and,
'pred2' denotes the predicted purlin deflection by reconstructed pressure histories.

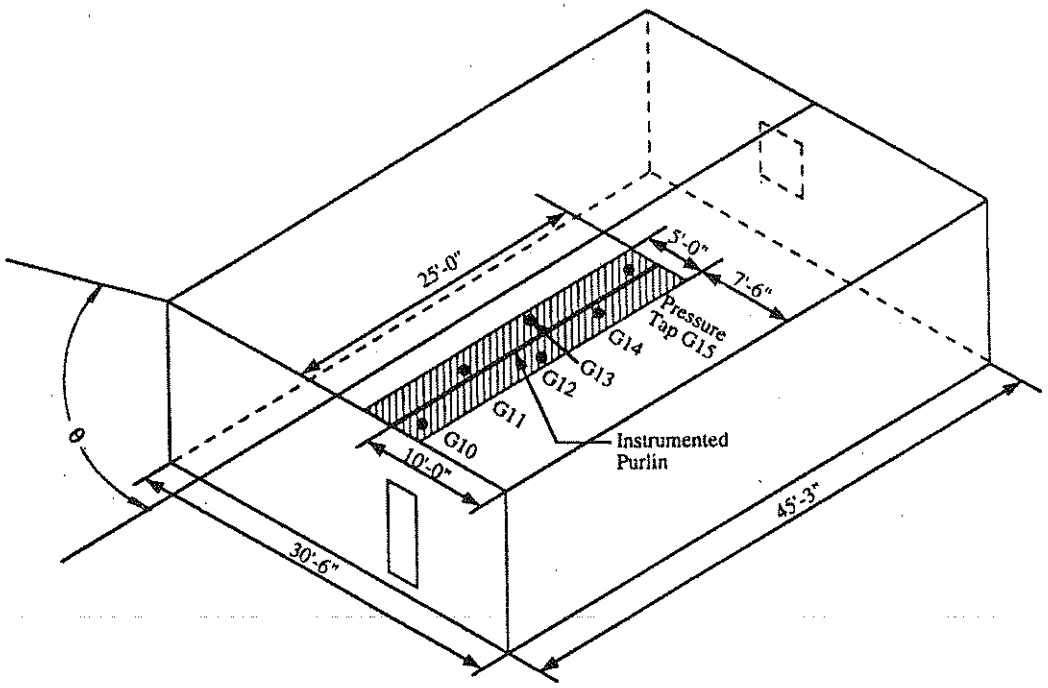

Figure 1. Location of the purlin and the pressure tap designation (Bhavaraju, 1993)

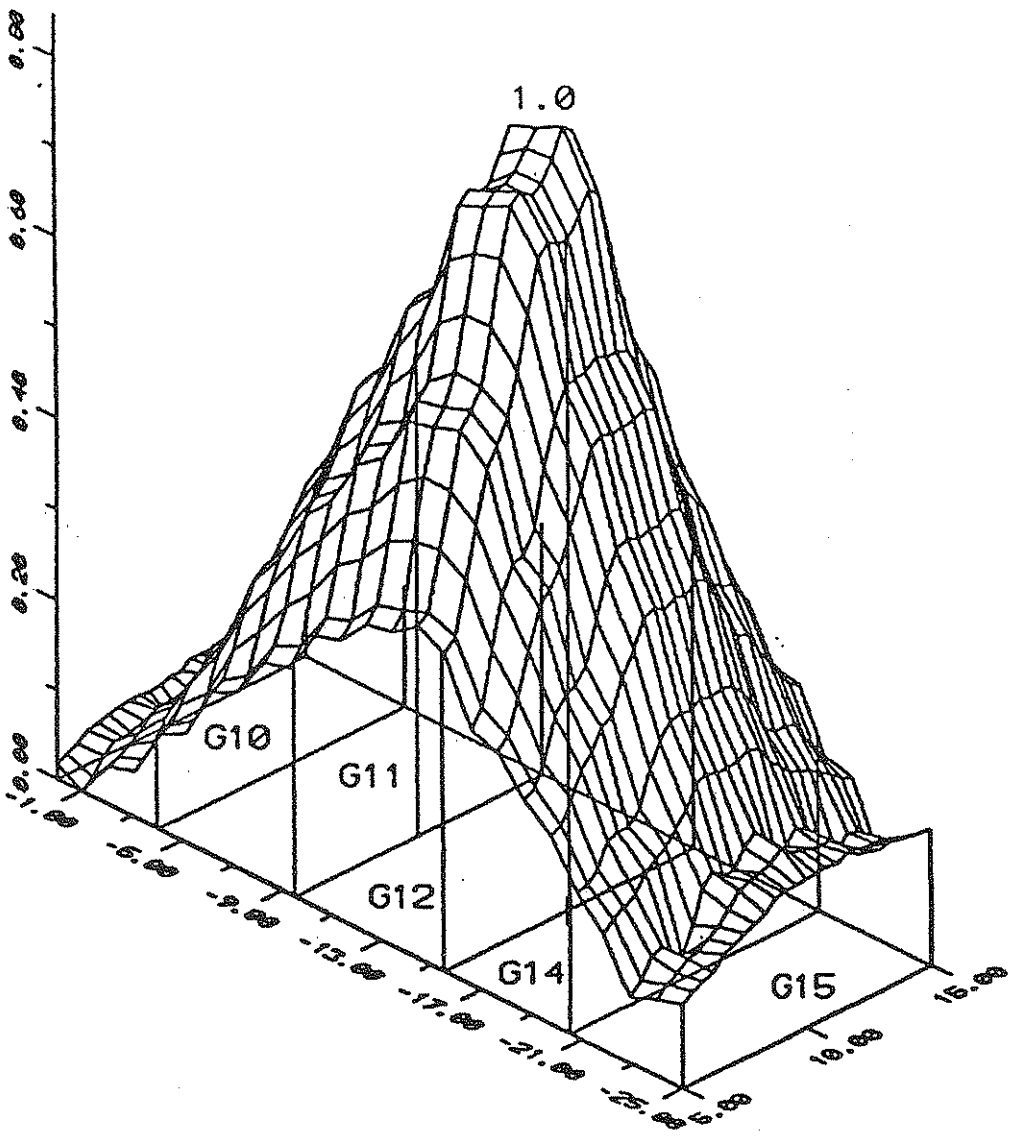

Figure 2. Static influence coefficient surface (Bhavaraju, 1993)

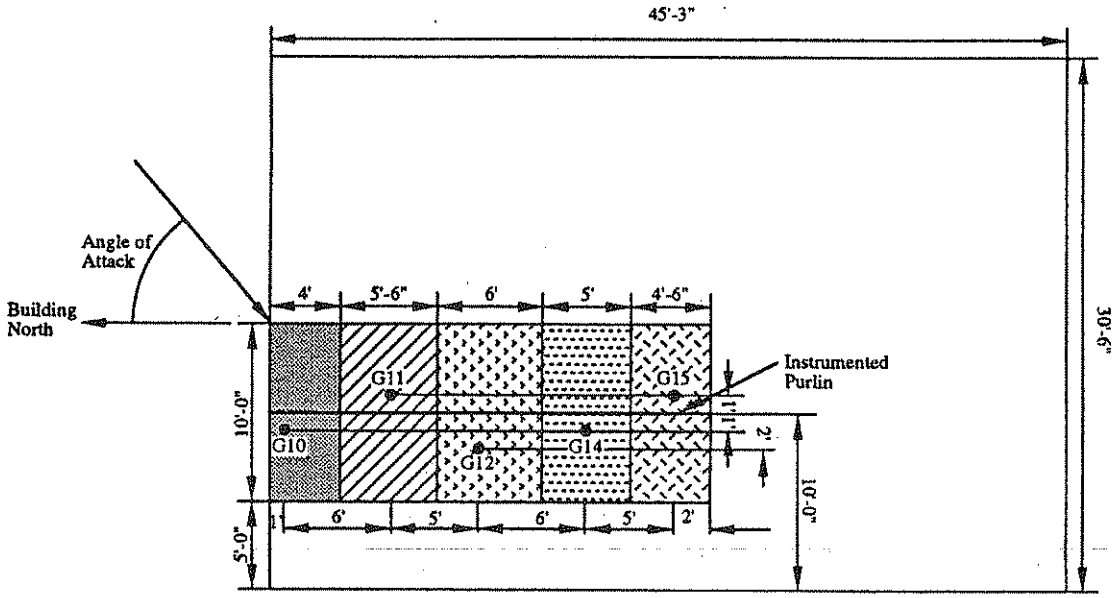

Figure 3. The effective area of pressure taps (Bhavaraju, 1993)

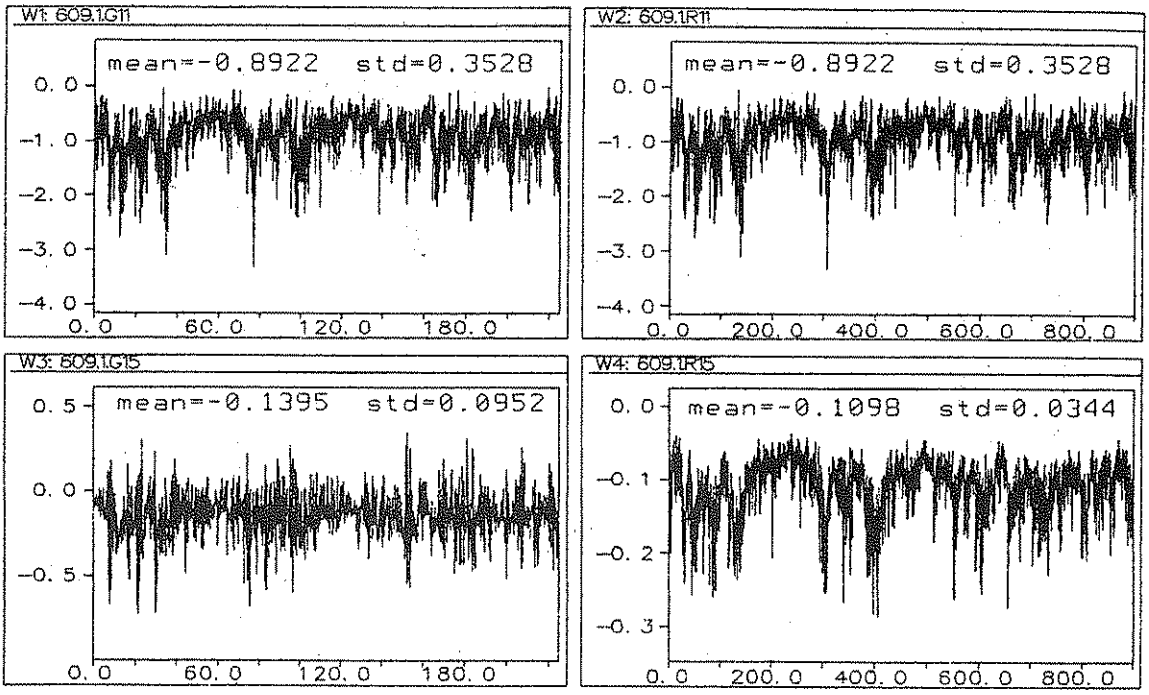

Figure 4. Comparison of original and reconstructed pressure histories

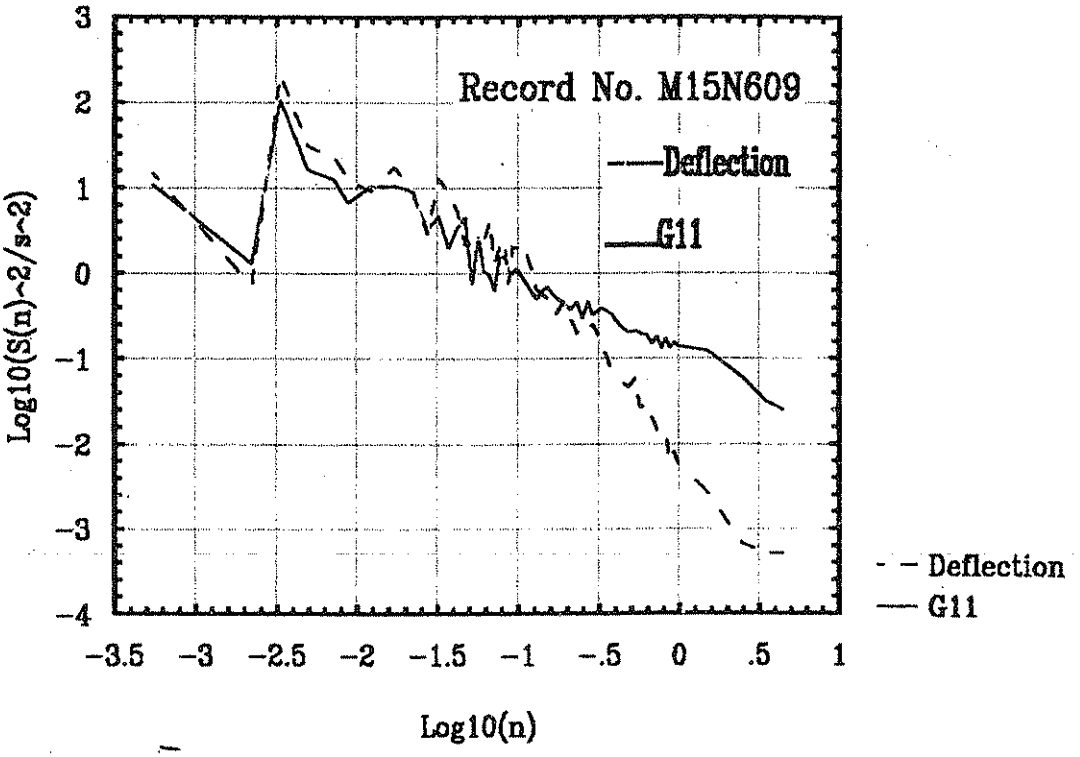

Figure 5. Comparison of normalized spectral density functions (M15N609)

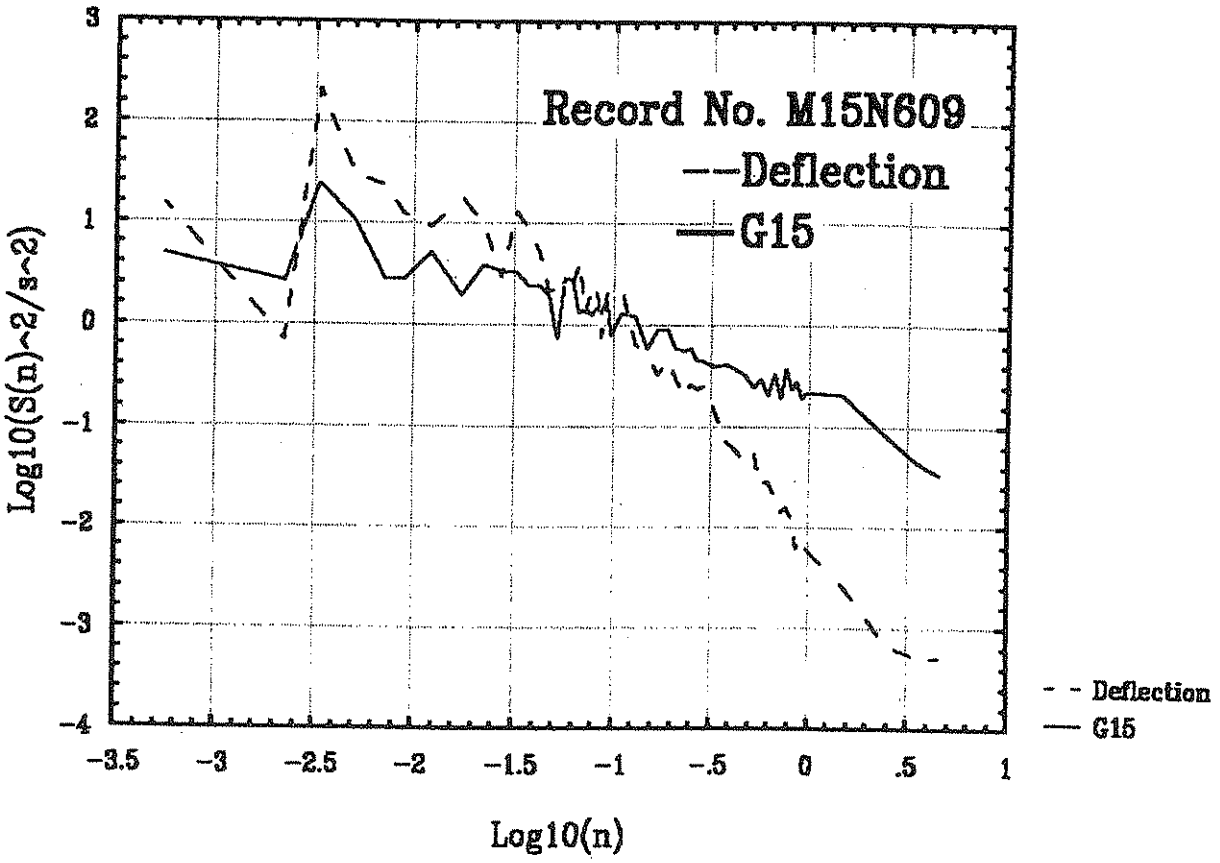

Figure 6. Comparison of normalized spectral density functions (M15N609)